Aerodynamic and Aeroacustic experimental investigation of a three propellers DEP configuration

De Paola E.[1], Camussi R.[1], Stoica L. G.[1], Di Marco A.[1] and Capobianchi G.[1]

[1]Department of Civil, Computer Science and Aeronautical Technologies Engineering
elisa.depaola@uniroma3.it

Abstract

With the development of new paradigms in urban air mobility, both the scientific community and the industry have increasingly focused on sustainable solutions such as distributed propulsion. Consequently, there has been a growing need to investigate the effects associated with these new configurations. The conducted study is part of the H2020 CS2 European project VENUS, which investigates methodologies and tools to enable a concurrent design approach for both the aerodynamics and aeroacoustics of aircraft employing distributed electric propulsion. Specifically, a 3D wing model, featuring a flap and powered by three electric motor-driven propellers, underwent a comprehensive testing campaign in the large-scale, low-speed, acoustically-treated wind tunnel of Pininfarina, Turin (Italy). A wide range of parameters was systematically varied and studied, including the blade pitch angle, the angle of attack, flap configurations for take-off and landing, phase shifts between propellers, and different relative distances both between the propellers themselves and with respect to the wing body. The experimental tests comprise both measurements of acoustics, such as beamforming and directivity analysis, and aerodynamics, through forces and wall pressure characteristics. This article provides an overview of the wind tunnel test results and the insights gained regarding the phenomena that occur for different DEP solutions. The main objective of this research is to assess potential optimal DEP configurations based on the aerodynamic and aeroacoustic performances exploited.

1 Introduction

Accompanying the ongoing surge in demand for civil aviation, the last decade has seen a remarkably swift evolution of Urban Air Mobility (UAM), Vertical Take-Off and Landing (VTOL) Personal Aerial Vehicles (PAVs), and Air Taxis. This paradigm shift aims to fulfill stringent objectives in efficiency, emissions reduction, noise mitigation, and maneuverability. Despite commendable advancements aligning with the objectives outlined in [12] and considerable efforts have been focused on reducing the environmental footprint of conventional aircraft, innovative designs and technologies are necessary to achieve goals regarding chemical and acoustic emissions. In this context, the aviation industry's pursuit of sustainable solutions has led to a notable exploration of distributed electric propulsion (DEP) as a transformative technology since it refers to a system where thrust is generated by an array of electrical engines positioned across the vehicle and able to significantly reduce fuel consumption and emissions. This configuration is expected to enhance the overall efficiency, capabilities, and performance of the air vehicle [15, 22], enhancing the system's aerodynamic performance by increasing lift and reducing induced drag through interactions between propeller wakes and the wing itself [16, 19]. However, while DEP offers promising advancements in fuel efficiency and reduced carbon emissions, it also introduces a nuanced challenge: the impact of noise associated with the distributed propulsors. The distributed nature of electric propulsion, involving multiple smaller propellers distributed across the wings, fuselage, or other parts of the aircraft, has the potential to create unique acoustic challenges. Traditional aircraft noise concerns primarily revolve around engines situated in specific locations, but DEP configurations introduce new considerations related to the acoustic interaction of multiple propellers. Indeed, the geometric configuration and synchronization of the rotors, along with their proximity to critical airframe components such as wings and flaps, can influence the overall noise signature. The distinctive noise sources in DEP configurations are often associated with the interaction between the propeller wake and the

aerodynamic surfaces of the aircraft. The ongoing research in this area underscores the commitment to shaping a future where sustainable aviation includes environmental responsibility and a quieter and more harmonious coexistence with communities surrounding airports. Efforts to address these noise challenges involve a multidisciplinary approach, integrating advancements in aerodynamics, aeroacoustics, and propulsion technology. A significant body of literature delves into the preliminary design, initial sizing of propulsive devices [15, 6, 14, 17], and the aerodynamic and aeroacoustic performances of such concepts [9, 13]. Focusing on the latter, accurate characterization of aerodynamic interactions among configuration components is vital, as these interactions strongly influence the aerodynamic performance and acoustic emissions of multi-rotor wing-mounted propulsive systems [4, 8, 21]. Given the limited literature on the subject, including [23], [7], [11], [10], to support the design of DP configurations, a deeper investigation into these aerodynamic and aeroacoustic interaction effects becomes crucial. Thus, while progress has been made in understanding the role of aerodynamic interactions in system performance, a straightforward procedure to identify optimal installation parameters for minimizing acoustic emissions while optimizing aerodynamic performance is still lacking.

The EU-funded VENUS project aims to contribute valuable insights into the aforementioned challenge through dedicated experimental wind tunnel tests, with the outcomes being the central focus of this study. Further information on the project can be found in [20] and on the official project website. Given the complexities of implementing hybrid/electrical distributed propulsion, especially as aircraft range and size increase, the initial application of this technology is expected to be in short-range Regional Aircraft, which served as a reference in defining the model tested in the wind tunnel. Information is sourced from public domain data [3], integrated with considerations for hybrid-electrical propulsion. During the design, efforts were made to minimize the tip Mach number and mitigate noise impact [5]. The model, composed of a wing with a movable flap and three propellers with their nacelles, underwent an experimental test campaign at the large-scale, low-speed, acoustically-treated wind tunnel of Pininfarina, Turin (Italy). The modularity of the model allowed several geometrical configurations since each propeller (and its nacelle) could be moved, independently from the others, both in the streamwise and in the spanwise directions. The phase of the rotors could be controlled as well, and several phase amplitudes, including an uncontrolled case, were tested. The model was instrumented with several pressure taps and microphones flush-mounted on the wing surface to measure the static and fluctuating wall pressure respectively. Moreover, the facility is equipped with both planar and linear microphone arrays, used for the beamforming and noise directivity analysis. A 6-component balance was adopted to measure the global aerodynamic forces and moments. The working parameters were selected to reproduce realistic conditions in terms of advance ratio and thrust coefficient. Specifically, the rotational speed of the propellers was fixed to 3300 rpm, and the free stream flow speed to 20 m/s. Eight geometrical configurations have been tested, corresponding to eight different positions of the propellers in the streamwise and spanwise directions. In each configuration, the Angle of Attack (AoA) was varied from -1° to 11° and the flap inclination was adjusted in three positions in order to reproduce cruise, take-off, and landing conditions. Further details about the experimental setup and the test plan are given in Section II whereas the most relevant results are presented in Section III. Conclusions and final remarks are described in Sec. IV.

2 Experimental set-up and test plan

The experimental test campaign was conducted at the Pininfarina Aerodynamic and Aeroacoustic Research Center in Turin, Italy. The semi-cylindrical open jet wind tunnel has a collector of radius 3 m, a test section of 8m x 9.6 m x 4.2 m, and is driven by a 29-bladed fan. The tunnel produces a uniform velocity flow, which varies by only 0.5% over the area of the test section. A wing scale model with a 1:3.6 ratio and equipped with three identical co-rotating propellers was installed in the wind tunnel test section, Fig. 1. This scaling corresponds to a full-scale scenario with thrust evenly distributed between the Distributed Electric Propulsion (DEP) and the main propeller. The main model dimensions are summarized in Table 1. The three electrically driven propellers are four-bladed

	Full scale	Model 1:3.6
Prop diameter [m]	2	0.556
Wing chord [m]	2.285	0.635
U_∞ [m/s]	63	20
rpm	2500	3300

Table 1: Full scale and model characteristics.

rotors, with each blade mounted at a pitch angle of 17°, a value that allows for maximum thrust. An appropriate

acoustic treatment of the wind tunnel reduces the background noise to 68.5 dBA at a flow velocity of 100 km/h (28 m/s) and 77.7 dBA at 140 km/h (39 m/s), measured out of the flow. The wind tunnel is equipped with three spiral microphone arrays (a lateral, a top, and a frontal array) for precise source localization, and a far-field linear one for the analysis of the polar directivity (refer to Fig. 1). The top array, depicted in green in Fig. 1, is placed at the ceiling of the WT at an offset of X = 3.175 m, Y = 0 m, Z = 4 m from the WT frame of reference at a fixed position. It is composed of 78 B&K 4951 type microphones disposed on a wheel of 3 m diameter. The lateral array, the blue one in Fig. 1, is positioned broadside at a distance of Y = 4.2 m and the center of the array is located at X=3.675 m and Z=1.7 m. It is composed of 66 B&K 4951 type microphones disposed on a half-wheel of 3 m diameter. The frontal array, magenta in Fig. 1 and composed of 15 B&K 4189 type microphones, is placed upstream of the blade plane at an offset of X=0.05 m, Y=0 m, Z=3.719 m from the wind tunnel frame of reference and it is rotated with respect to the Y-direction (on XZ plane) by about 50°. The linear array, cyan in Fig. 1, of 11 B&K 4951 type microphones is centered on the blade plane covering polar angles from approximatively θ_m=30° to θ_m=150° about the blade plane in baseline configuration. Due to the wide range of configurations tested, it was not possible to re-align this array exactly with the front blade plane for each wing geometry and AoA setting. All the microphone arrays are outside the WT flow. Microphone signals were acquired simultaneously at a data rate of 65536 Hz for 20s duration.

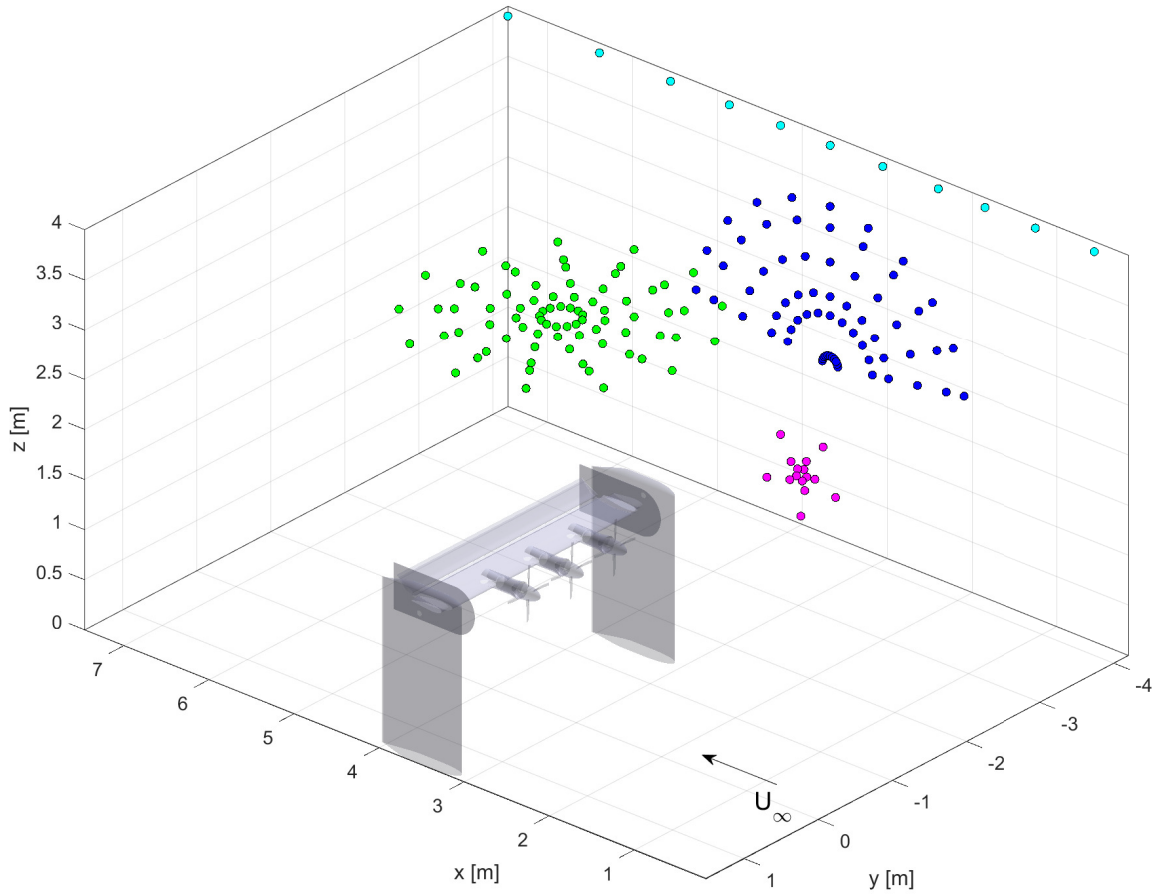

Figure 1: Installed model and microphone arrays Pininfarina wind tunnel.

Operating at a wind tunnel speed of 20 m/s and a propeller speed of 3300 rpm, the resulting advance ratio is $J = 0.63$. This value is representative of full-scale applications, as it was obtained by scaling down the realistic configuration to maintain consistent thrust requirements under typical operating conditions. To simulate 2D conditions, the model is positioned horizontally, and the wing is inverted, as depicted in Fig. 1. The experimental setup for the wind tunnel test campaign includes a wide range of instrumentation on the model, in particular:

- an Angle of Attack (AoA) mechanism specifically designed to facilitate the adjustment of the Angle of Attack.

- Rotary encoders and accelerometers strategically placed to enable precise speed and rotor phase control of the propellers.
- Global balance connected to the model struts: The model struts are linked to the global balance beneath the test section floor, enabling the measurement of aerodynamic forces.
- Pressure taps and microphones mounted both on the flap and the wing. The flap and wing are extensively instrumented with 96 pressure taps and 44 microphones strategically located (as illustrated in Fig. 2). The pressure taps, acquired by two Chell μDAQ 64-channel pressure scanners, capture the static pressure distribution while the fluctuating pressure is recorded using Knowles FG-23629-P16 capsule electret microphones. These measurements are essential to investigate the interaction between the propeller wake and the wing and flap, providing insights into their roles in the noise generation process.

This sophisticated instrumentation setup ensures a comprehensive examination of the aerodynamic and aeroacoustic aspects during the wind tunnel tests, offering valuable data to identify the configuration with the best aerodynamic and aeroacoustic performance.

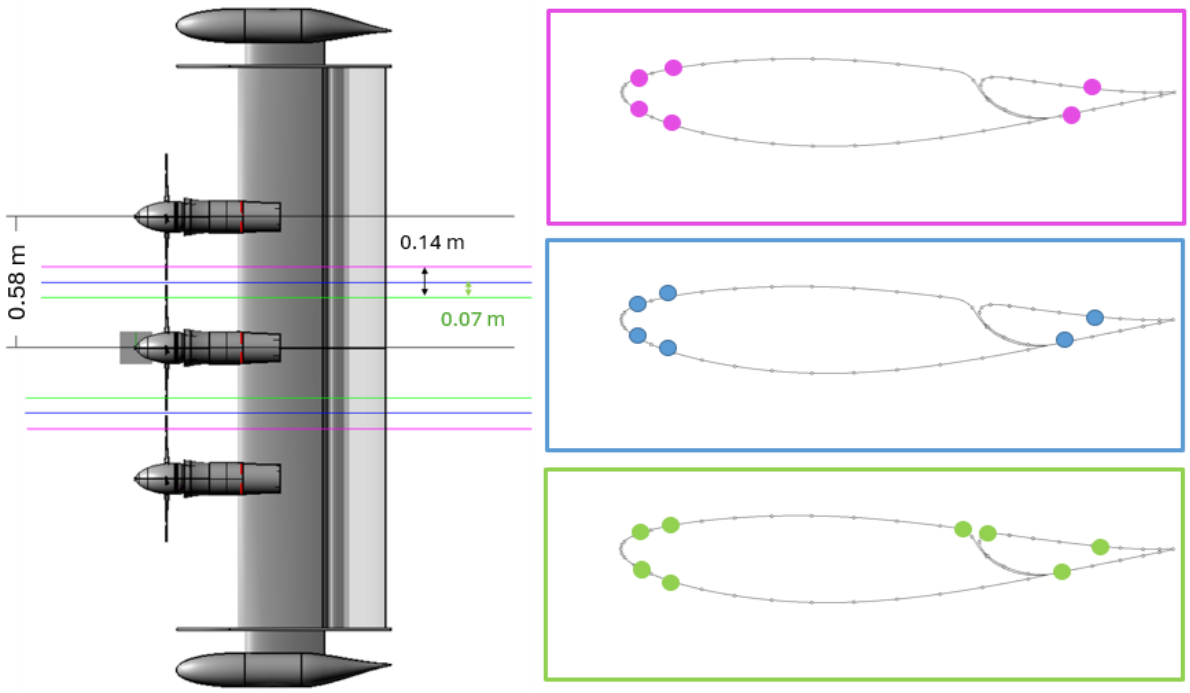

Figure 2: Steady (small dots) and unsteady (colored dots) pressure sensors positions.

The wind tunnel tests entail the systematic variation of distances between the outer propellers and the central one (ΔY) and the distances with respect to the wing (ΔX), resulting in eight distinct combinations denoted as XY. The distance with respect to the wing (ΔX) is confined to three values: baseline (X_{BL}=449 mm), X_{BL}-60 mm, and X_{BL}+60 mm, facilitated by specifically designed removable inserts. The hub-to-hub distance (ΔY) between the outer nacelles and the central one can continuously vary between 694 mm and 547 mm, with the baseline value set at 583.8 mm (refer to Fig. 3). The tested configurations are summarized in Table 2.

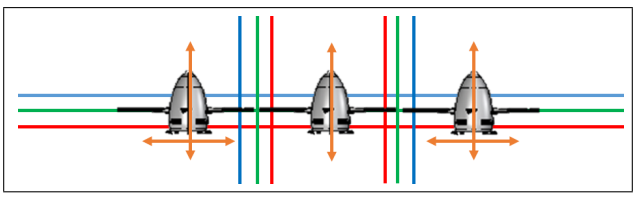

Figure 3: Sketch of the nacelles movements ΔX and ΔY; green=BL, red=closest, blue=farthest positions.

Name	$\Delta Y[m]$	$\Delta X_{Left}[m]$	$\Delta X_{Central}[m]$	$\Delta X_{Right}[m]$
XY1	0.5838	0.449	0.449	0.449
XY2	0.5838	0.509	0.509	0.509
XY3	0.5838	0.509	0.389	0.509
XY4	0.5838	0.389	0.509	0.389
XY5	0.5838	0.449	0.509	0.449
XY6	0.5838	0.449	0.389	0.449
XY10	0.547	0.509	0.389	0.509
XY11	0.547	0.389	0.509	0.389

Table 2: Geometrical configuration tested.

The investigation covers both take-off (TO) and landing (LA) configurations, involving two distinct flap settings: $\delta = 20°$ and $\delta = 35°$ respectively. The phase shift between the propellers is meticulously controlled via a PID controller. For each geometrical configuration, two phase angles are tested. Each test point comprises an angle of attack sweep ranging from $-1°$ to $11°$ in increments of $1°$. The varied parameters during the tests are summarized in Table 3. Before commencing the tests, the pitch angle was calibrated to ensure that the nominal thrust was achieved within the wind tunnel measurements. All the meticulous analyses conducted before the experimental campaign ensure the accuracy and reliability of the wind tunnel tests.

Parameter	Value
AoA (α)	$-1° \rightarrow 11°$
Flap angle (δ)	$20°$ (TO), $35°$ (LA)
Phase shift ($\Delta\varphi$)	$0°, 35°$
ΔX, ΔY	XY1 $\rightarrow$ XY11

Table 3: Parameters varied during wind tunnel tests.

3 Experimental results

In this section, the results of the WT tests are presented initially in terms of force and moment coefficients, followed by the study of aeroacoustic effects, with the ultimate goal of evaluating the best geometric configuration in terms of both aerodynamic and acoustic performance. Furthermore, some insight into the static and fluctuating wall pressure trends is provided.

3.1 Aerodynamic results

To identify the configuration with the best aerodynamic performance, the effect of the geometrical position of the three propellers is investigated in terms of forces and moments. Given the impossibility of having a direct measure of the thrust, this force has been measured as the difference between the total measured drag force with propellers running and the drag of the model without installing the rotors in the same configuration. Once the drag difference is calculated the thrust coefficient is obtained through the:

$$\mathrm{C}_T = \frac{X_{withprop} - X_{withoutprop}}{\rho n^2 D^4} \tag{1}$$

Where ρ is the density measured in the WT for each test, n is the number of revolutions per second, D is the diameter of the propeller and X is the total force acquired by the WT balance in the x-direction. The trends of the thrust coefficients as a function of the angle of attack α are illustrated in Fig. 4 for all tested geometric configurations. In general, the C_T decreases as the angle of attack α increases, and no significant effect of the rotor phasing can be detected; therefore, for brevity, the trends are only presented for zero-degree phase shifts, ($\Delta\phi = 0°$), where both in take-off (TO) and landing (LA), the higher C_T coefficients are exhibited, suggesting that the phase shift between the blades induces a slightly detrimental effect on the propulsive force. As expected, the lower thrusts are obtained in the landing (LA) configuration as the model with the flap rotated at $35°$ exerts more drag than in the take-off case. In TO, the configuration XY10, with staggered rotors, provides the greatest

thrusts at low AoA ($\alpha < 6°$). On the contrary, in LA, this configuration exhibits the worst performances, Figure 4. This could be explained by the fact that the wake of the rotors impacting the wing is more turbulent and already distorted when the propellers are staggered, dissipating more rapidly as the flow passes over the wing. By the way, his effect becomes more critical when the angle of attack is increased. During take-off, the flap deflection angle is lower compared to landing, and this appears to be beneficial not only in terms of reducing aerodynamic resistance but also in the flow separation effect and potential disturbances introduced by the presence of the gap between the wing and flap, which compound with those due to the rotor wake and result in more detrimental effects on thrust during landing rather than take-off. As a general observation, none of the tested configurations stands out among the others as the best in terms of propulsive force, indicating that geometry does not seem to significantly influence this parameter. From the analysis of aerodynamic polars presented in Fig. 5 and 6 the following considerations

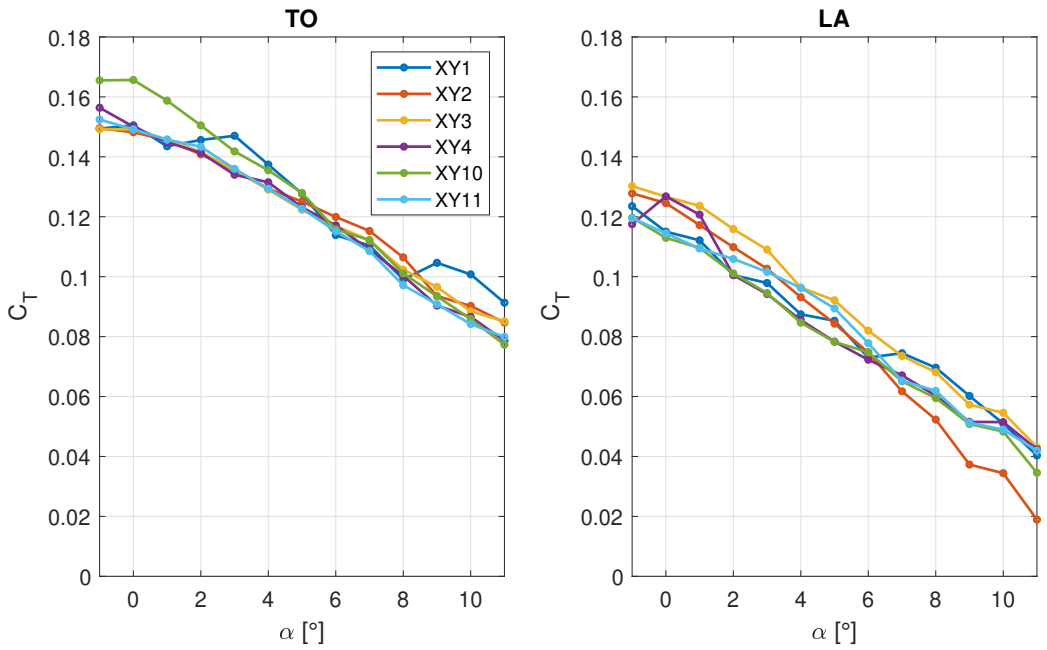

Figure 4: DEP thrust coefficients for all the geometrical combinations in TO (left) and LA (right) at $0°$ phase shift.

are derived. In TO, the different propeller positioning seems not to affect the aerodynamic forces whereas a certain impact is achieved on the moment coefficient. The lowest moment coefficient corresponds to the staggered propeller arrangements XY10 and XY11. This is because the wake effects of the three co-rotating rotors have a lesser impact on the moment since the vortex structures are less coherent compared to configurations with rotors placed at a certain tip distance from each other. In LA, a slight effect on the lift is observed identifying the XY2 configuration, with the three rotors positioned closest to the wing's leading edge, as the most aerodynamically efficient and the XY10 as the worst, Figure 6. Indeed, when the rotors are installed as close as possible to the wing, their wakes exhibit greater coherence, resulting in a beneficial effect on lift.

According to the analyses conducted on the global dimensions, the configuration with the rotor discs positioned in the proximity of the wing emerges as the most aerodynamically efficient. In spite of that, to better understand the aerodynamics of the various configurations and confirm what was previously highlighted, the trends of static and fluctuating pressures measured on the wing were studied. The former analysis did not provide additional information, except for the identification of a strong asymmetry of the loads in the spanwise direction due to the rotation of the wake downstream of the rotors, in agreement with what was predicted by numerical simulations, [20]. For brevity, the results obtained are not shown, on the other hand, a brief description of the analysis of the wall pressure fluctuations is presented being more effective in identifying the best geometric configurations. In particular, the Cp_{rms} was evaluated for each flush-mounted sensor as follows:

$$Cp_{rms} = \frac{\sigma_p}{\frac{1}{2}\rho U^2} \tag{2}$$

where σ_p represents the standard deviation of the pressure and ρ the fluid density. Results are illustrated referring

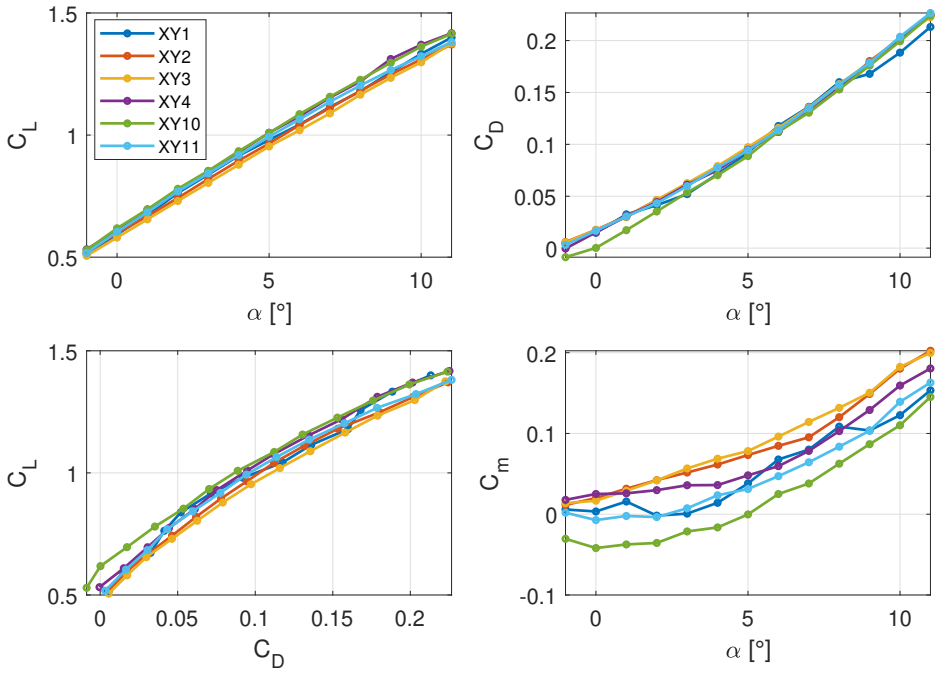

Figure 5: Effect on the polars of the nacelles geometrical combinations in TO for $0°$ phase shift.

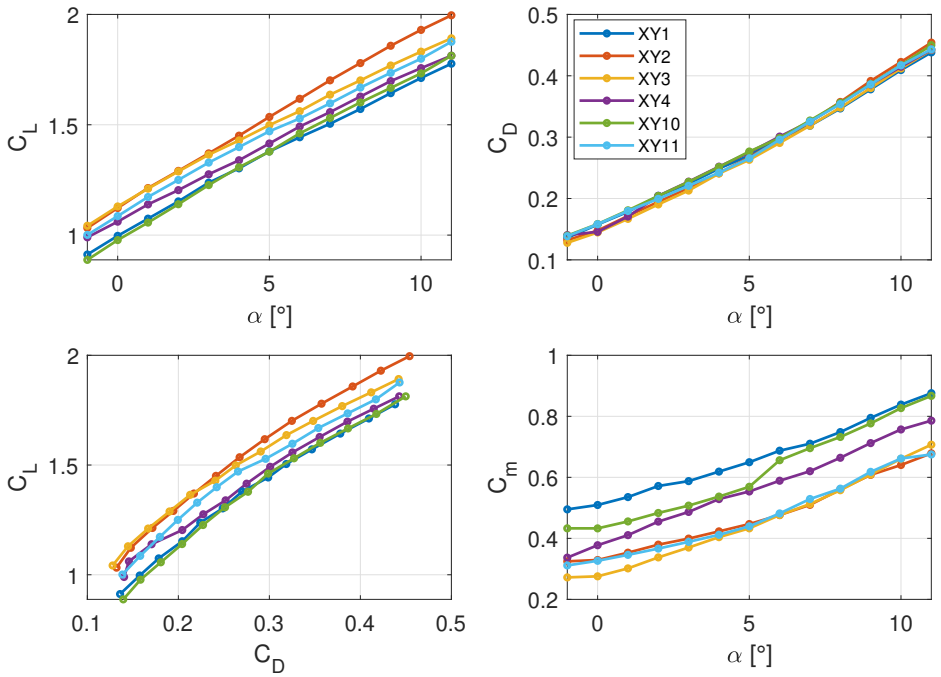

Figure 6: Effect on the polars of the nacelles geometrical combinations in LA for $0°$ phase shift.

to the sensor positions reported in Fig. 2 and Fig. 7 both for the wing and the flap. The Cp_{rms} values measured by each transducer are plotted for all the geometrical configurations at the angle of attack $\alpha = 0°$ relating to each of the installation lines, (denoted by green, blue, and magenta lines), positioned both to the right and left side of the central propeller. Since similar results are obtained for the blue and magenta lines, for brevity, only the results for

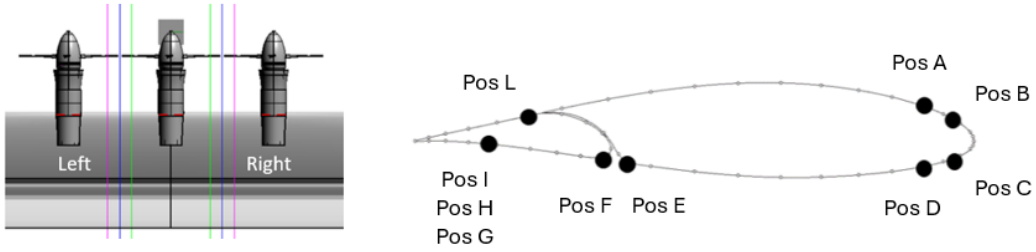

Figure 7: Knowles microphone locations.

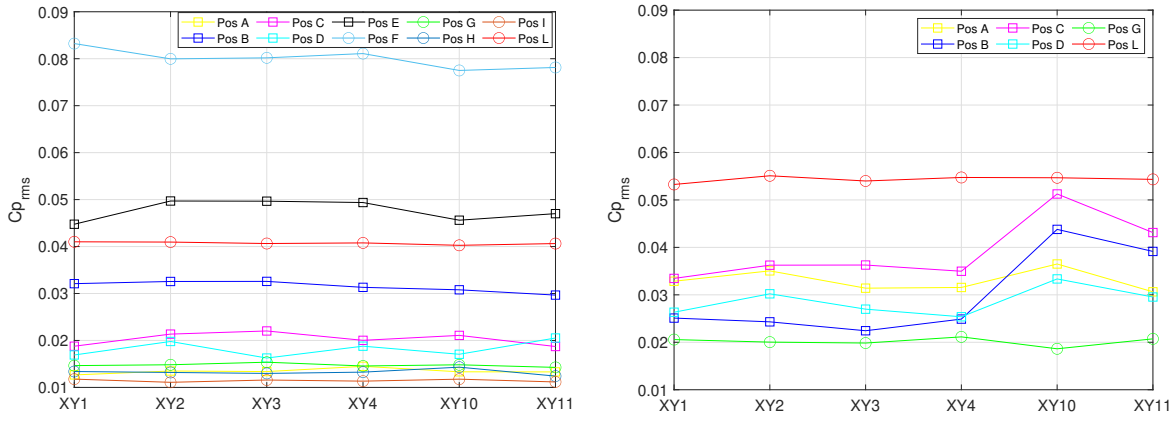

(a) Green line - Left side

(b) Blue line - Left side

(c) Green line - Right side

(d) Blue line - Right side

Figure 8: Cp_{rms} comparison between all the geometrical configuration, $\Delta\phi = 0°$, $\alpha = 0°$.

the blue line are presented in Fig. 8, along with the values for the green line. It should be noted that the two sensors placed on the pressure side in the gap between the wing and flap were installed only on the green line, closer to the central rotor. Additionally, at the position indicated as Pos G, two additional transducers, Pos H and Pos I, were mounted, having the same chordwise coordinate but slightly translated in the spanwise direction, allowing for a statistical correlation analysis, which is not addressed in this study. Comparing the results obtained to the right and left side of the central propeller, the asymmetry of the load distribution on the wing surface is confirmed in all the rotor arrangements tested. The greater variations are generally obtained in the positions closest to the central propeller, green line, and the highest pressure fluctuations are found at the gap between the flap and the wing, corresponding to Pos E and Pos F in Fig. 8. In terms of geometrical configuration, the highest Cp_{rms} values

are obtained in the ones with staggered propellers, XY10 and XY11, more notably at the leading edge and closer to the blade tip, as shown in figure 8 by the sensors denoted as Pos A, Pos B, Pos C, and Pos D installed along the blue line, suggesting that such rotor positioning results in an increased load on the surface, making it less advisable in terms of performance. To conclude, an example of the spectra calculated for the sensors on the pressure side is provided in Figure 9, in which not only the harmonic content related to the presence of the rotors is clearly visible including in the signals from the sensors placed on the flap, but also an increase in energy due to the effect of the flap itself is denoted by the trends depicted with the yellow and orange line in the figure. This effect has been attributed to the increase in the broadband component due to the presence of the gap between the main body and the high-lift device.

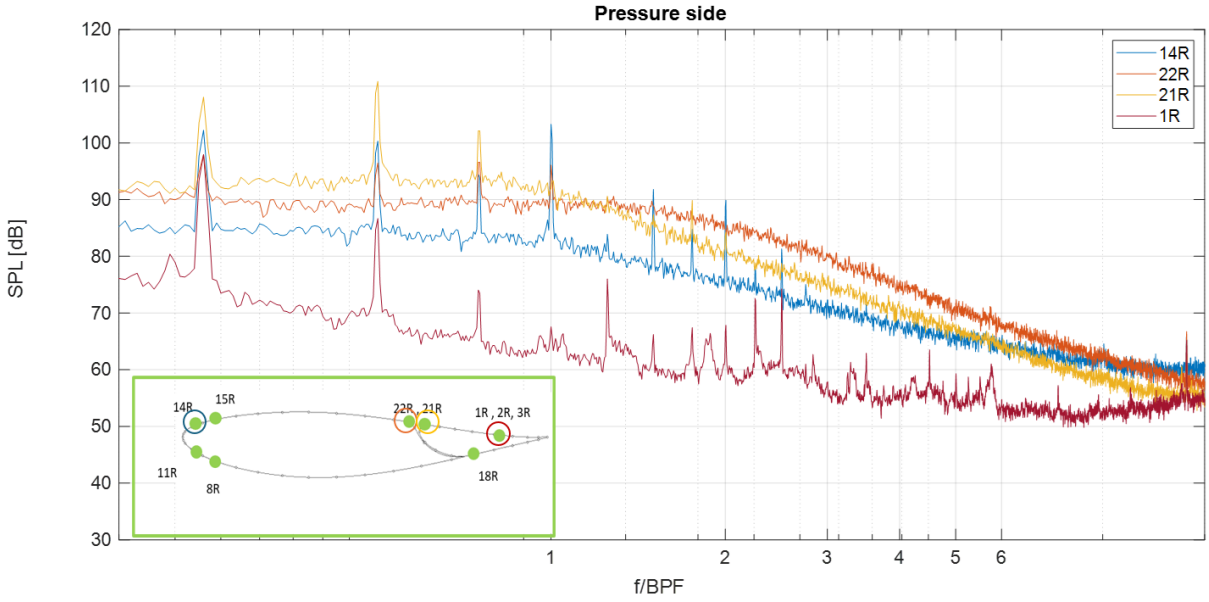

Figure 9: Pressure spectra of selected Knowles positions, TO configuration, $\Delta\phi = 0°, \alpha = 0°$.

3.2 Aeroacoustic results

The aeroacoustic investigation initially involved evaluating the noise source maps from the top, lateral, and front arrays using the conventional beamforming algorithm (CB) in the frequency domain [1, 18].

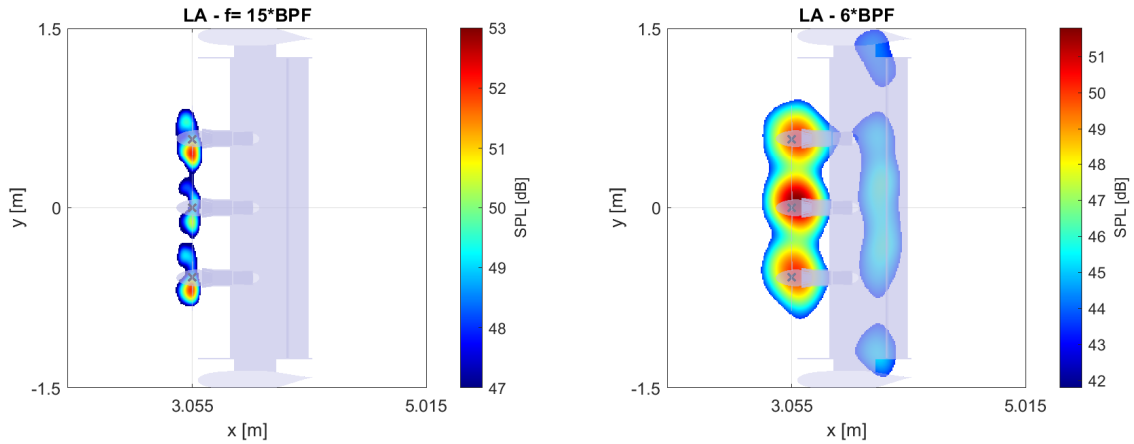

(a) $f = 15 * BPF$ (b) $f = 6 * BPF$

Figure 10: Beamforming map referred to the baseline configuration, top array, $\Delta\phi = 0°$, $\alpha = 0°$.

The analysis is concentrated on a single frequency corresponding to the 15th BPF at approximately 3300 Hz to achieve a good spatial resolution. However, no relevant information is obtained unless qualitatively individualizing the major noise sources mainly localized at the rotors, and therefore, the maps cannot be used to individualize acoustically optimal configurations. An example of the maps obtained from the top array is shown in Fig. 10a, while in Fig. 10b, the map calculated for the same case at a lower frequency, 6*BPF, is illustrated. The loss of spatial resolution is noted, but it is possible to highlight the presence of an additional noise source represented precisely by the gap between the wing and the flap, as identified by the study of wall pressure fluctuations.

The acoustic directivity of the model for the different DEP configurations is then presented in terms of OASPL measure by the WT linear array and corrected taking into account some wind tunnel effects such as the presence of a shear layer due to the jet, the atmospheric attenuation, and the spherical spreading of the noise radiation from the source, according to the literature [2]. To identify the arrangement with the best acoustic performance, the results obtained at zero phase shift and zero incidence are presented for both take-off (TO) and landing (LA), in Fig. 11.

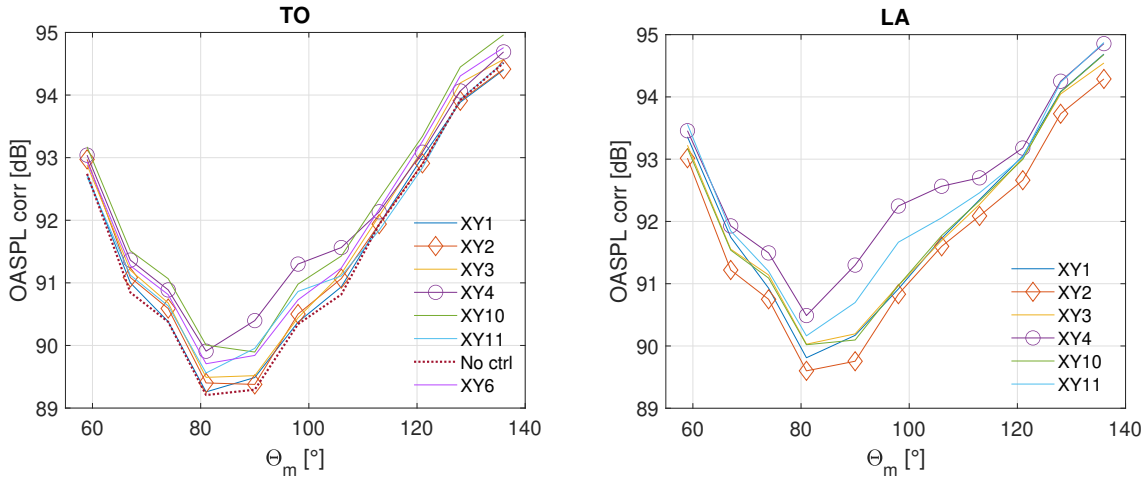

Figure 11: Acoustic directivity of the model in different DEP configurations, $\Delta\phi = 0°, \alpha = 0°$.

The optimal acoustic configuration is observed to be XY2, with all rotors positioned at the nearest distance from the wing. This finding aligns with the results obtained from the aerodynamics study. The physical explanation for this outcome is believed by the authors to lie in the fact that when the rotors are farther from the wing, the behavior is more similar to isolated propellers, and the wakes appear more turbulent when interacting with the main body. Conversely, when the rotors are positioned closer to the leading edge, the related vortical structures maintain greater coherence as they pass over the wing, resulting in a lower broadband noise component. In both take-off and landing scenarios, the least favorable geometric configuration, in terms of OASPL, is identified as XY4 (only the central nacelle close to the wing). It is demonstrated that, during take-off, the configuration without any phase control yields the lowest noise levels; however, this aspect was not tested during landing.

Considering this, the influence of the phase shift between the three propellers is also verified. What is noticeable from the comparison of the spectra evaluated both for $\Delta\phi = 0°$ and $\Delta\phi = 35°$, is a phase shift effect on the amplitude of the peaks in the spectrum relative to the shaft frequency and its harmonics, which proves to be beneficial in terms of reducing the harmonic peaks due to the presence of the rotors. An example of the results obtained, referring to the baseline configuration (XY1) at zero incidences, is presented in Fig. 12, where a comparison of the spectra measured by a microphone representative of the community noise and positioned in the top array directly above the rotor disk of the central propeller is illustrated. Furthermore, to inspect possible optimal $\Delta\phi$ values for minimizing the noise emissions, a phase sweep test was performed at $0°$ angle of attack in the baseline configuration at landing. The outcome is presented in terms of SPL at the first BPF in Fig. 13 referring both to the microphone in the top array comparable to the effect on community noise, Fig. 13a, and to a microphone at the location of the rotor disks in the linear array, $\theta_m = 90°$, in Fig. 13b. In the former case, the trend clearly confirms that $35°$ is the optimal phase angle shift for reducing the noise emissions, as indicated by the preliminary numerical simulations [20], while from the trend shown in Fig. 13b, slightly different minimum values of $\Delta\phi$ are obtained, still suggesting a more noticeable noise reduction when the phase shift angles is between $\Delta\phi = 30°$ and $\Delta\phi = 70°$.

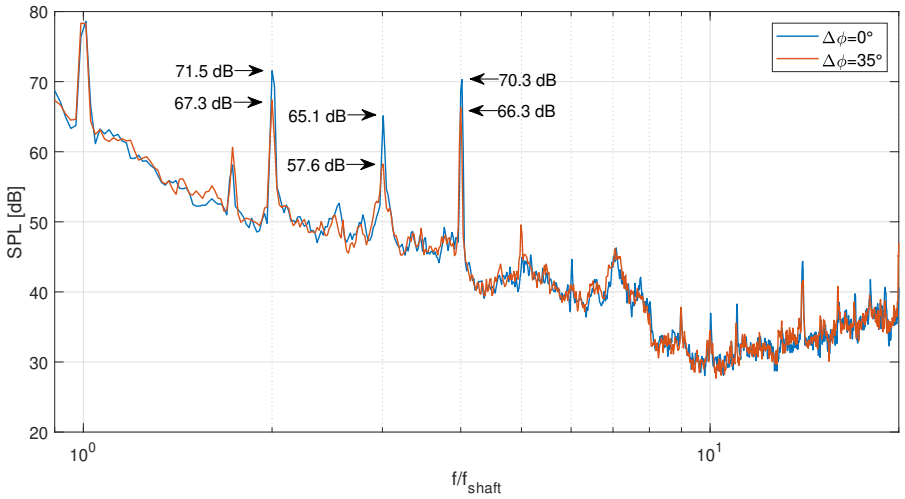

Figure 12: Different phase angles spectra comparison in the baseline configuration.

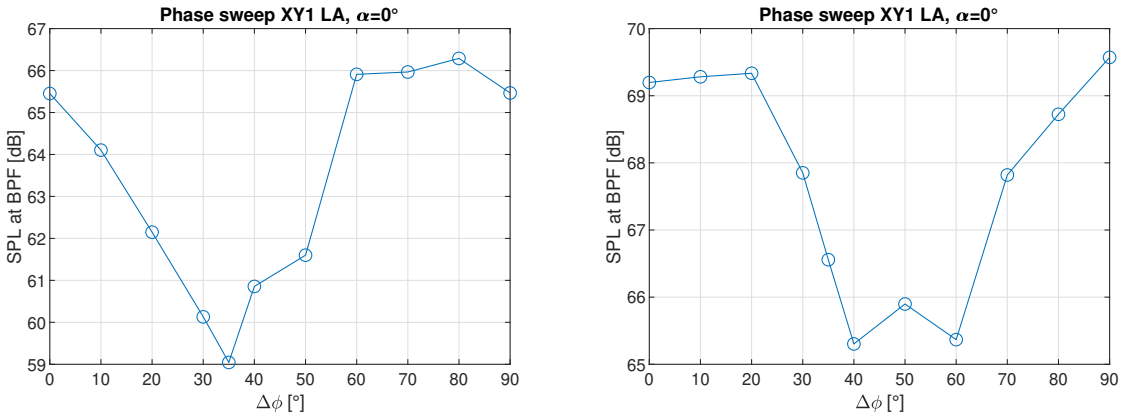

(a) Top array

(b) Linear array

Figure 13: SPL at the BPF for different phase shifts in the baseline configuration: a) mic over the central propeller from the top array; b) mic $\theta_m = 90°$ linear array.

4 Conclusions

The VENUS project aims to investigate distributed electric propulsion configurations using experimental as well as high-fidelity numerical data, defining an open test case for the scientific community. To define a realistic application, a 48-passenger regional aircraft with a typical mission of 200 Nm was considered in the preliminary design of the model. It was assumed that thrust is provided entirely by DEP system during take-off and landing. The blade geometry was optimized to have a uniform velocity in the propeller inflow. Blades were manufactured and tested to verify the natural frequencies from the Campbell diagram. The purpose of this study is to present the results obtained from the experimental test campaign conducted in the Pininfarina wind tunnel, with the ultimate goal of identifying the geometric configuration with the best aerodynamic and aeroacoustic performance. The wind tunnel tests were performed at a wind tunnel speed of 20 m/s and a propeller speed of 3300 rpm, resulting in an advance ratio of J = 0.63. The model was positioned horizontally to simulate 2D conditions. The extensive set of measurements included forces acting on the model, propeller torque, and far-field aeroacoustic data using the four microphone arrays installed in the Pininfarina wind tunnel. Steady and unsteady pressures were strategically measured along the wing and flap to inspect the interaction effects between the propeller wake and the wing. Various parameters were considered, such as angle of attack, flap angle, hub-to-hub distances between propellers, their distance with respect to the wing, and the phase shift between propellers. Key findings from the tests are as follows:

- In take-off (TO), different propeller positions did not significantly impact aerodynamic forces and the lowest

moment coefficient occurred with the staggered propeller positioning XY10 and XY11.

- In landing (LA), only a slight effect on the lift was observed, identifying the XY2 configuration as the most aerodynamically efficient and XY10 as the least.
- Both in TO and LA, higher thrust coefficients were observed when the rotors were in phase ($\Delta\phi = 0°$), suggesting a penalizing effect on thrust when the rotors were out of phase ($\Delta\phi = 35°$).
- In LA, staggered configurations provided the worst thrust performances and induced a distribution of loads on the surface that is more significant compared to other configurations, as evidenced by the analysis of wall pressure fluctuations.
- No significant effect of parameters on noise source localization (beamforming maps), which primarily originated from the rotors. For landing, a minor additional noise source was identified at frequencies below 15 times the Blade Passage Frequency (BPF), related to the gap between the wing and flap.
- A phase shift effect was highlighted when $\Delta\phi = 35°$, proved to be beneficial in terms of reducing the harmonic peaks due to the presence of the rotors.
- Comparing the polar directivities retrieved by the linear array, the optimal acoustic configuration is observed to be XY2, with all rotors positioned at the nearest distance from the wing.
- Aerodynamic and aeroacoustic parameters aligned with preliminary numerical optimization.

The analysis performed has successfully met the objective of assessing potential optimal DEP configurations, offering valuable insights into the performance of these innovative solutions. In particular, a comprehensive comparison of aerodynamic and aeroacoustic data highlighted that the XY2 configuration, with three rotors placed closer to the wing, demonstrated the best overall performance and it was found that maintaining a relative rotor phase shift of $35°$ allows for reducing the noise emissions of the studied solutions. As part of the European VENUS project, all the data and documents produced constitute an open test case accessible to the entire scientific community through a direct request to the authors.

Acknowledgments

This work is part of the project VENUS (inVestigation of distributEd propulsion Noise and its mitigation through wind tUnnel experiments and numerical Simulations), which has received funding from the Clean Sky 2 Joint Undertaking under the European Union's Horizon 2020 research and innovation program under grant agreement 886019. Acknowledgements are due to the partners involved, particularly the Italian Aerospace Research Center (CIRA) who managed the propulsive system, optimized the propeller, and conducted CFD simulations. NHOE srl, responsible for automation and control systems on the model, Eligio Re Fraschini SpA, involved in manufacturing the model, wind tunnel installation, and IBK Innovation who handled model design.

References

[1] C.S. Allen, T.J. Mueller, W.K. Blake, R.P. Dougherty, D. Lynch, P.T. Soderman, and J.R. Underbrink. *Aeroacoustic Measurements*. Experimental Fluid Mechanics. Springer Berlin Heidelberg, 2013.

[2] R.K. Amiet. Refraction of sound by a shear layer. *Journal of Sound and Vibration*, 58(4):467–482, 1978.

[3] ATR and aircraft. Atr 42-600 aircraft. Last accessed 2023.

[4] Giovanni Bernardini, Francesco Centracchio, Massimo Gennaretti, Umberto Iemma, Claudio Pasquali, Caterina Poggi, Monica Rossetti, and Jacopo Serafini. Numerical characterisation of the aeroacoustic signature of propeller arrays for distributed electric propulsion. *Applied Sciences*, 10(8):2643, 2020.

[5] Jeffrey J Berton and Douglas M Nark. Low-noise operating mode for propeller-driven electric airplanes. *Journal of aircraft*, 56(4):1708–1714, 2019.

[6] Nicholas K Borer, Michael D Patterson, Jeffrey K Viken, Mark D Moore, JoeBen Bevirt, Alex M Stoll, and Andrew R Gibson. Design and performance of the nasa sceptor distributed electric propulsion flight demonstrator. In *16th AIAA Aviation Technology, Integration, and Operations Conference*, page 3920, 2016.

[7] Huanxian Bu, Han Wu, Celia Bertin, Yi Fang, and Siyang Zhong. Aerodynamic and acoustic measurements of dual small-scale propellers. *Journal of Sound and Vibration*, 511:116330, 2021.

[8] Elisa De Paola, Alessandro Di Marco, Luana Georgiana Stoica, Leonardo Falcini, and Roberto Camussi. Experimental investigation on a side-by-side twin rotor system in pusher configuration. *INTER-NOISE and NOISE-CON Congress and Conference Proceedings*, 265(2):5862–5872, 2023.

[9] Reynard de Vries, Nando van Arnhem, Tomas Sinnige, Roelof Vos, and Leo LM Veldhuis. Aerodynamic interaction between propellers of a distributed-propulsion system in forward flight. *Aerospace Science and Technology*, 118:107009, 2021.

[10] Alessandro Di Marco, Roberto Camussi, Elisa de Paola, Luana Georgiana Stoica, et al. Experimental investigation of the aeroacoustic interaction effects of installed pusher propellers. In *28th AIAA/CEAS Aeroacoustics 2022 Conference*, page 2833, 2022.

[11] Jernej Drofelnik, Matej Andrejasic, Blaz Mocan, Tadej Kosel, et al. Measurement and modelling of aeroacoustic installation effects in tractor and pusher propeller architectures. In *AIAA AVIATION FORUM*, page 2301, 2021.

[12] EC. Flightpath 2050, europe's vision for aviation. Technical report, European Commission, 2011.

[13] Antoine Hajczak, Julien Christophe, Cansev Y Kucukosman, and Christophe F Schram. Numerical parametric investigation of aeroacoustic installation effects in a distributed electric propulsion system. In *28th AIAA/CEAS Aeroacoustics 2022 Conference*, page 3006, 2022.

[14] Jean Hermetz, Michael Ridel, and Carsten Doll. Distributed electric propulsion for small business aircraft a concept-plane for key-technologies investigations. In *ICAS 2016*, 2016.

[15] Hyun D Kim, Aaron T Perry, and Phillip J Ansell. A review of distributed electric propulsion concepts for air vehicle technology. In *AIAA/IEEE Electric Aircraft Technologies Symp. (EATS)*, pages 1–21. IEEE, 2018.

[16] Emanuel A Marcus, Reynard de Vries, Akshay Raju Kulkarni, and Leo L Veldhuis. Aerodynamic investigation of an over-the-wing propeller for distributed propulsion. In *2018 AIAA Aerospace Sciences Meeting*, page 2053, 2018.

[17] Michael D Patterson, Joseph M Derlaga, and Nicholas K Borer. High-lift propeller system configuration selection for nasa's sceptor distributed electric propulsion flight demonstrator. In *16th AIAA Aviation Technology, Integration, and Operations Conference*, page 3922, 2016.

[18] Ennes Sarradj and Gert Herold. A python framework for microphone array data processing. *Applied Acoustics*, 116:50–58, 2017.

[19] Tomas Sinnige, Nando van Arnhem, Tom CA Stokkermans, Georg Eitelberg, and Leo LM Veldhuis. Wingtip-mounted propellers: Aerodynamic analysis of interaction effects and comparison with conventional layout. *Journal of Aircraft*, 56(1):295–312, 2019.

[20] Luana Georgiana Stoica, Alessandro Di Marco, Roberto Camussi, Elisa De Paola, Umberto Iemma, Lorenzo Burghignoli, Giorgio Palma, Nicola Paletta, Nikos Pepelas, Jacopo Beretta, Antonio Visingardi, Antonio Pagano, Giuseppe Mingione, Carmelo Izzo, Giovanni Andreutti, Mattia Barbarino, Domenico Quagliarella, Pier Luigi Vitagliano, Roberto Pasta, Luca Flamini, and Fabio Rusconi. Venus project: Investigation of distributed propulsion noise and its mitigation through wind tunnel experiments and numerical simulations. In *Forum Acusticum Conference 2023, Turin, Italy*, 2023.

[21] Austin David Thai, Elisa De Paola, Alessandro Di Marco, Luana Georgiana Stoica, Roberto Camussi, Roberto Tron, and Sheryl Marie Grace. Experimental and computational aeroacoustic investigation of small rotor interactions in hover. *Applied Sciences*, 11(21), 2021.

[22] Jérôme Thauvin, Guillaume Barraud, Marc Budinger, Xavier Roboam, Dimitri Leray, and Bruno Sareni. Hybrid regional aircraft: A comparative review of new potentials enabled by electric power. In *52nd AIAA/SAE/ASEE joint propulsion conference*, page 4612, 2016.

[23] Teng Zhou and Ryu Fattah. Tonal noise acoustic interaction characteristics of multi-rotor vehicles. In *23rd AIAA/CEAS Aeroacoustics Conference*, page 4054, 2017.